Multiport Analysis of Arbitrary Circular-Rod Insets in Rectangular Waveguide by the Generalized Admittance Matrix

Gian Guido Gentili

***Abstract*—An original generalized-admittance-matrix (GAM) approach for the analysis of multiport junctions in rectangular waveguide having an arbitrary circular-rod inset is presented in this paper. The method is based on an efficient computation of the GAM for the blocks that compose the structure. The efficiency is due to the fact that, for each block, the full three-dimensional GAM is obtained by solving a set of uncoupled two-dimensional problems. The accuracy and efficiency of the method developed have been assessed by comparing the results obtained with some measured data and with data obtained by the finite-element method.**

***Index Terms*—Combline filters, generalized admittance matrix.**

I. Introduction

CIRCULAR rod insets in rectangular waveguides and/or resonators have been used quite often in both "classic" and more recent filter applications. They are used in combline filters, where facing rods are used, one as part of the resonators, the other acting as a tuning element [1], [2], and matching or tuning by circular screws is used in T-junctions or cross junctions, with applications to diplexers and phase shifters. Finally, they can simply represent tuning screws and inductive or capacitive posts in rectangular waveguides filters [3], [4]. In all these applications, when the post height is smaller than the waveguide height, the analysis is not trivial because the problem is three-dimensional (3-D) and the simultaneous presence of circular- and rectangular-shape elements makes the application of standard modal approaches difficult. Quite recently, the two-port case (posts in a waveguide) were analyzed by Zaki *et al.* [1] by a radial mode-matching approach. The two-port case is interesting in the frame of combline filters applications because the filter can be realized by cascading basic cells of multimode two-port networks. However, the simple cascade connection limits the analysis to the case of filters where only direct coupling between adjacent resonators is used. The important case of meander combline filters, implementing arbitrary transmission zeros, cannot be analyzed by connecting two-port networks. That class of filters, whose importance is rapidly growing in mobile communications, requires additional couplings and a more complex topology. In this paper, we use the generalized-admittance-matrix (GAM) concept to analyze general multiport structures (up to four ports) with arbitrary circular rod insets (see Fig. 1). The advantages of the GAM are flexibility (simple manipulation of rather complex geometries by recursive submatrix computation), relatively small matrix size, and direct computation with no large matrix inversion. This last feature is attractive in filter applications since the GAMs of the basic cells can be directly connected without the need to compute the generalized scattering matrix (GSM). This latter can be computed only as a final step and for reduced-size matrices involving only accessible modes. The formulation developed in this paper is based on a particular decomposition of the structure allowing the transformation from the original 3-D problem to a set of simpler uncoupled two-dimensional (2-D) problems. For these, efficient routines have been developed, leading to a remarkable speed of analysis for the entire structure.

The paper is organized as follows. The formulation is discussed in detail in Section II and then several numerical and measured results are presented. The comparison with measurements allows to point out the good accuracy of the method developed even with a moderate number of basis functions.

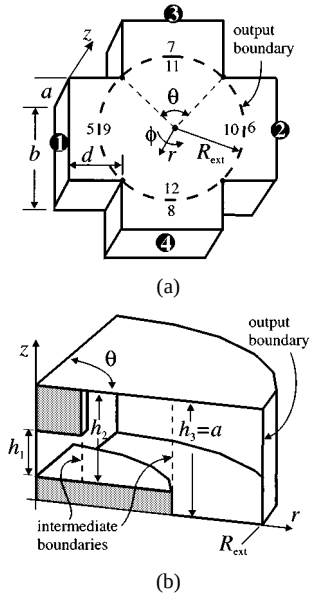

Fig. 1 . Port numbering for a generic four-port structure and radial geometry of an arbitrary circular rod inset.

Manuscript received February 23, 2000; revised September 29, 2000. This work was supported by the Centro Studie Laboratorie Telecommunicazioni S.p.A. under a contract.

The author is with the Centro Studi per le Telecomunicazioni Spaziali, National Research Council, Dipartimento di Elettronica e Informazione, Politecnico di Milano, I-20133 Milan, Italy (e-mail: gentili@elet.polimi.it).

Publisher Item Identifier S 0018-9480(01)06138-5.

II. Formulation

A. General Remarks

The two main blocks the structure has been divided into are a cylindrical and transition region. The latter has been analyzed by a very efficient approach discussed in previous papers [5], [6]. When applied to the problem discussed in this paper, the method developed in [5] allows an interesting further advantage, consisting in an unusual shift in the reference planes, leading to a sort of desegmentation of the structure.

A radial GAM approach has been developed to analyze the cylindrical inner region, representing a general coaxial/circular resonator to which rectangular waveguides are connected. An example of a four-port structure is shown in Fig. 1, where the inner fictitious cylindrical region is denoted by a dashed line. This figure actually represents a four-port multimode structure obtained by combining an inner four-port structure (representing the generic circular rod inset and up to the fictitious circular boundary) with four transition regions representing the rectangular-to-curved surface connection. The transition regions has been analyzed with a very efficient procedure that computes the full 3-D GAM by solving several 2-D problems, and a similar decomposition can be adopted also when computing the GAM for the internal cylindrical region. In this case, the full 3-D GAM is obtained by computing several 2-D GAM, constituting the radial GAMs defined for a specified value of the azimuthal index m.

B. Block Decomposition

The structure is divided into an internal part (comprising the arbitrary coaxial loading and up to ports 9–12 in Fig. 1) and two or more *transition regions* [a transition region is the physical structure between rectangular waveguide ports (1–4), and curved ports (5–8)]. Connection between the blocks is carried out by directly connecting the GAMs. The general "connection problem" can be represented by assuming that a generic device A, whose GAM is $\mathbf{Y}^A$, must be connected to a generic device B, whose GAM is $\mathbf{Y}^B$ through a common subset of ports. Matrices $\mathbf{Y}^A$ and $\mathbf{Y}^B$ can be partitioned into submatrices relative to the common subset of ports as follows:

$$\mathbf{Y}^A = \begin{bmatrix} \mathbf{Y}^A_{pp} & \mathbf{Y}^A_{pq} \\ \mathbf{Y}^A_{qp} & \mathbf{Y}^A_{qq} \end{bmatrix} \quad \mathbf{Y}^B = \begin{bmatrix} \mathbf{Y}^B_{rr} & \mathbf{Y}^B_{rs} \\ \mathbf{Y}^B_{sr} & \mathbf{Y}^B_{ss} \end{bmatrix} \tag{1}$$

where it is assumed that the ports subset q of device A is connected to the ports subset r of device B. After the connection, device C results, whose GAM is whose ports are the ports subset p of device A and the ports subset s of device B. One finds

$$\begin{aligned} \mathbf{Y}^C &= \begin{bmatrix} \mathbf{Y}^C_{pp} & \mathbf{Y}^C_{ps} \\ \mathbf{Y}^C_{sp} & \mathbf{Y}^C_{ss} \end{bmatrix} \\ &= \begin{bmatrix} \mathbf{Y}^A_{pp} - \mathbf{Y}^A_{pq}\mathbf{Z}\mathbf{Y}^A_{qp} & -\mathbf{Y}^A_{pq}\mathbf{Z}\mathbf{Y}^B_{rs} \\ -\mathbf{Y}^B_{sr}\mathbf{Z}\mathbf{Y}^A_{qp} & \mathbf{Y}^B_{ss} - \mathbf{Y}^B_{sr}\mathbf{Z}\mathbf{Y}^B_{rs} \end{bmatrix} \end{aligned} \tag{2}$$

where $\mathbf{Z} = (\mathbf{Y}^A_{qq} + \mathbf{Y}^B_{rr})^{-1}$.

Since the transition regions are uncoupled from one another, the connection of one region at a time is convenient since it corresponds to smaller matrix inversions.

We can now specialize to the computation of GAMs for the two sub-blocks.

C. Transition Region

The transition regions connect the external ports (1–4 in Fig. 1) to the internal fictitious boundary (defined by ports 9–12). The reference planes are defined by parameter d in Fig. 1. The single transition region can be efficiently analyzed, as in [5], by a GAM approach based on a 2-D contour integral defined for each value of the discrete parameter k_z (the wavenumber along coordinate z). For any fixed k_z, the 2-D contour integral is obtained from Green's second identity

$$\begin{aligned} \oint_S \varphi \frac{\partial W^\varphi}{\partial n}\, dl' &= \oint_S W^\varphi \frac{\partial \varphi}{\partial n}\, dl' \\ \oint_C \psi \frac{\partial W^\psi}{\partial n}\, dl' &= \oint_C W^\psi \frac{\partial \psi}{\partial n}\, dl' \end{aligned} \tag{3}$$

where φ and ψ are Hertz-type potentials, W^φ, W^ψ are suitable testing functions (solutions of Helmholtz equation), C is the 2-D boundary of the transition region, and $\partial/\partial n$ indicates derivative in the normal direction. The potentials and their normal derivatives are expanded on the boundary in a set of basis function and the following set of testing function is used:

$$\begin{aligned} W^\varphi &= \cos\frac{m\pi}{b}\, y \cdot e^{\mp\gamma_m x}, \qquad m = 0, \ldots, M \\ W^\psi &= \sin\frac{m\pi}{b}\, y \cdot e^{\mp\gamma_m x}, \qquad m = 1, \ldots, M \end{aligned} \tag{4}$$

where $\gamma_m = \sqrt{(m\pi/a)^2 + (n\pi/b)^2 - k^2}$ and $k = \omega\sqrt{\mu\varepsilon}$. Owing to the wise choice of the testing functions, the GAM relative to all desired modes is obtained in less than a second on a simple personal computer (PC).

An further interesting feature of the method in [5] is the possibility to choose parameter d quite arbitrarily. In our case, the most advantageous choice is to set $d = 0$. In this case, the connection between the four transition regions and the internal fictitious boundary shifts the reference planes *inside* the structure, yielding an output boundary (ports 1–4) square in shape. This corresponds to a *desegmentation* of the structure [7]. The advantage of the method developed in [5] is that the shift in the reference planes is embedded in the method (d is a parameter arbitrarily chosen in the method) and no further manipulation is needed (the alternative way to shift the reference planes directly on the GAM is to connect waveguide sections of positive/negative length).

D. Internal Arbitrary Coaxial Loading and the Radial GAM

We use a cylindrical coordinate system (r, ϕ, z) and make constant reference to Fig. 1. The internal part of the structure, up to the fictitious output boundary $r = R_{\text{ext}}$, is analyzed by a new radial GAM approach. The GAM approach makes use of a dyadic Green's function of the admittance type $\overline{\mathbf{G}}$ yielding the magnetic field for any given electric field applied on the

boundary of a generic coaxial-type region defined by an inner radius $R_{\rm in}$ and an outer radius $R_{\rm out}$. As an example, a three-region internal structure is shown in Fig. 1. In order to compute the GAM for a generic closed region, one must define a set of basis functions to expand the electric field $\{\mathbf{f}_\eta\}$ and a corresponding set of testing functions to test the magnetic field $\{\mathbf{n}\times\mathbf{f}_\eta\}$. The generic element $Y(\xi,\,\eta)$ of the GAM is defined as

$$Y(\xi,\,\eta)=\int_S \mathbf{n}\times\mathbf{f}_\xi(\mathbf{r})\cdot\int_S \overline{\mathbf{G}}(\mathbf{r},\,\mathbf{r}')\cdot\mathbf{f}_\eta(\mathbf{r}')\,dS'\,dS \quad (5)$$

where $\mathbf{f}_\eta$ is the ηth basis function, $\mathbf{n}$ is the inward normal unit vector, S is a closed surface, and $dS(dS')$ is the elementary surface element. The definition in (5), combined with the use of normalized basis functions, leads to a symmetric GAM (the proof allows from the reciprocity theorem), which is a useful feature in the analysis. Function $\overline{\mathbf{G}}$ has been obtained, after some lengthy manipulations, by a radial-wave expansion and its transverse (to $\mathbf{n}$) part takes on the following form:

$$\begin{aligned}\overline{\mathbf{G}}(\mathbf{r},\,\mathbf{r}')=&\,G_{\phi\phi}(z,\,\phi,\,z',\,\phi')\mathbf{u}_\phi\mathbf{u}_\phi+G_{\phi z}(z,\,\phi,\,z',\,\phi')\mathbf{u}_\phi\mathbf{u}_z\\&+G_{z\phi}(z,\,\phi,\,z',\phi')\mathbf{u}_z\mathbf{u}_\phi+G_{zz}(z,\,\phi,\,z',\,\phi')\mathbf{u}_z\mathbf{u}_z\end{aligned} \quad (6)$$

where

$$G_{\phi z}=\sum_{m=0}^{\infty}\cos m(\phi-\phi')\sum_{n=0}^{\infty}g_{\phi z}^{m,\,n}\cos k_{zn}z\cos k_{zn}z' \quad (7)$$

$$G_{z\phi}=\sum_{m=0}^{\infty}\cos m(\phi-\phi')\sum_{n=0}^{\infty}g_{z\phi}^{m,\,n}\sin k_{zn}z\sin k_{zn}z' \quad (8)$$

$$G_{zz}=\sum_{m=0}^{\infty}\sin m(\phi-\phi')\sum_{n=0}^{\infty}g_{zz}^{m,\,n}\cos k_{zn}z\sin k_{zn}z' \quad (9)$$

$$G_{\phi\phi}=\sum_{m=0}^{\infty}\sin m(\phi-\phi')\sum_{n=0}^{\infty}g_{\phi\phi}^{m,\,n}\cos k_{zn}z\sin k_{zn}z'. \quad (10)$$

In (7)–(10), $k_{zn}=n\pi/h$, h is the generic coaxial cavity height (along z), and

$$g_{zz}^{m,\,n}=\frac{D_{m,\,n}mk_{zn}Z_{m,\,R_H}^{(F)}}{j\omega\mu R_E^2\partial_r Z_{m,\,R_E}^{(F)}} \quad (11)$$

$$g_{z\phi}^{m,\,n}=\frac{D_{m,\,n}m(k^2-k_{zn}^2)Z_{m,\,R_H}^{(F)}}{j\omega\mu R_E\partial_r Z_{m,\,R_E}^{(F)}} \quad (12)$$

$$\begin{aligned}g_{\phi z}^{m,\,n}=&-\frac{j\omega\varepsilon D_{m,\,n}\partial_r Z_{m,\,R_H}^{(A)}}{(k^2-k_{zn}^2)R_E Z_{m,\,R_E}^{(A)}}\\&-\frac{D_{m,\,n}m^2k_{zn}^2Z_{m,\,R_H}^{(F)}}{j\omega\mu R_H R_E^2(k^2-k_{zn}^2)\partial_r Z_{m,\,R_E}^{(F)}}\end{aligned} \quad (13)$$

$$g_{\phi\phi}^{m,\,n}=\frac{D_{m,\,n}mk_z Z_{m,\,R_H}^{(F)}}{j\omega\mu R_H R_E\partial_r Z_{m,\,R_E}^{(F)}}. \quad (14)$$

In (11)–(14), $D_{m,\,n}=\varepsilon_{m0}\varepsilon_{n0}/2\pi h$, $\varepsilon_{p0}=2-\delta_{p0}$, $k=\omega\sqrt{\mu\varepsilon}$, R_H is the radius where the magnetic field is computed, R_E is the radius where the electric field is applied, and ∂_r indicates the derivative with respect to r. Functions $Z_{m,\,R}^{(A)}$, $Z_{m,\,R}^{(F)}$ are the r-dependency of Hertz-like potentials. Setting $k_r=\sqrt{k^2-k_{zn}^2}$, a stable representation (that overcame numerical overflow/underflow errors) is as follows:

$$Z_{m,\,r}^{(A)}=\begin{cases}Y_m(k_r r)-J_m(k_r r)Y_m(k_r R_0)/J_m(k_r R_0),\\\quad\text{if } k_r \text{ is real}\\K_m(|k_r|r)-I_m(|k_r|r)\,K_m(|k_r|R_0)\,I_m(|k_r|R_0),\\\quad\text{if } k_r \text{ is imaginary}\end{cases} \quad (15)$$

$$Z_{m,\,r}^{(F)}=\begin{cases}Y_m(k_r r)-J_m(k_r r)Y_m'(k_r R_0)/J_m'(k_r R_0),\\\quad\text{if } k_r \text{ is real}\\K_m(|k_r|r)-I_m(|k_r|r)\,K_m'(|k_r|R_0)/I_m'(|k_r|R_0),\\\quad\text{if } k_r \text{ is imaginary}\end{cases} \quad (16)$$

where J_m, Y_m (I_m, K_m) are the standard (modified) Bessel's functions of order m of the first and second kinds, respectively, the prime ($'$) indicates derivative with respect to the argument, and R_0 is a radius where perfect-conductor boundary conditions are applied ($R_{\rm in}$ or $R_{\rm out}$). When the region is simply circular (no inner conductor), then $Z_{m,\,r}^{(A)}=Z_{m,\,r}^{(F)}=J_m(k_r r)$ or $I_m(|k_r|r)$ according to k_r.

A 2-D radial GAM is obtained by fixing parameter m (this corresponds to taking the inner sums in (7)–(10). Any circular rod configuration can be solved for fixed m by expanding the unknown along z only. The unknown is expanded on each intermediate boundary in Fig. 1 and up to the output boundary using a sinusoidal basis. By cascading radial GAMs (for fixed m) for each region, one gets the whole radial GAM representing the arbitrary rod configuration for any fixed m at the output radial boundary [the final GAM is obtained by a simple recursive procedure obtained from (2)]. Let us now indicate by $\mathbf{Y}^{(m)}$ the matrix thus obtained, and let its generic element be represented by $Y^{(m)}(p,\,q)$. Indexes p and q are related to the z-dependency only of basis and testing functions. Then let m'' and m' represent the indexes of the sinusoidal basis and testing functions along the curved ports 9–11 so that each basis function is associated with the index pair $(q,\,m'')$ and each testing function with pair $(p,\,m')$. Element $Y(p,\,m',\,q,\,m'')$ of the *final* GAM for the internal region at ports 9–11 in Fig. 1 can be expressed as

$$Y(p,\,m',\,q,\,m'')=\sum_{m=0}^{\infty}c^{(m)}(p,\,m')Y^{(m)}(p,\,q)c^{(m)}(q,\,m'') \quad (17)$$

where $c^{(m)}(q,\,m'')$ and $c^{(m)}(p,\,m')$ represent the frequency-independent projection coefficients linking the basis and testing functions defined on the ports to the corresponding functions defined on the *whole* external boundary. Note that the projections refer to *variable* ϕ only since the z-dependency is already included in $\mathbf{Y}^{(m)}$. Note also that this transformation is applied at the output boundary only, independent of the complexity of the internal cylindrical insets structure.

E. Two- and Four-Port Structures

The two-port case is analyzed by setting angle θ in Fig. 1 to 180° and by using two transition regions. The resulting geom-

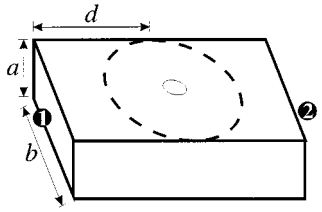

Fig. 2. Geometry and fictitious boundary for a two-port structure with an arbitrary circular rod inset.

etry is shown in Fig. 2. In this case, although one could still use $d = 0$ to fix the reference planes at the middle of the coaxial loading, any value can be used.

The three-port case is obtained by computing the whole GAM for the four-port case and by short circuiting one-ports (this correspond to extracting a $3N \times 3N$ submatrix from the $4N \times 4N$ GAM, N being the number of modes at each port). Also, in the case of a two-port structure with orthogonal ports (say, ports 1 and 3 in Fig. 1), the full four-port matrix is computed and the corresponding submatrix is then extracted.

In the case of a four-port device, as in Fig. 1, one can exploit the fourfold symmetry of the structure. By referring the GAM to the output curved ports using subscripts (9–11, as in Fig. 1), and by using the block circulant property of matrix $\mathbf{Y}$, one can express it as

$$\mathbf{Y} = \begin{bmatrix} \mathbf{Y}_{9,9} & \mathbf{Y}_{9,10} & \mathbf{Y}_{9,11} & \mathbf{Y}_{9,11}^T \\ \mathbf{Y}_{9,10}^T & \mathbf{Y}_{9,9} & \mathbf{Y}_{9,11}^T & \mathbf{Y}_{9,11} \\ \mathbf{Y}_{9,11}^T & \mathbf{Y}_{9,11} & \mathbf{Y}_{9,9} & \mathbf{Y}_{9,10} \\ \mathbf{Y}_{9,11} & \mathbf{Y}_{9,11}^T & \mathbf{Y}_{9,10}^T & \mathbf{Y}_{9,9} \end{bmatrix} \tag{18}$$

where superscript T indicates transposition. From (18), one can observe that only submatrices $\mathbf{Y}_{9,9}$, $\mathbf{Y}_{9,10}$, and $\mathbf{Y}_{9,11}$ must be computed.

III. Results and Convergence Discussion

The method developed has been applied to two-, three-, and four-port structures. For four-port (and three-port) structures, the algorithm runs slower than for two-port structures by a factor of about two. The CPU time for a two-port analysis, using 60 modes in rectangular waveguide was about 1 s/frequency point on a PC Pentium 350 MHz. The convergence was observed to be quite good even with a moderate number of basis functions (along z and ϕ on the intermediate boundaries in Fig. 1). Convergence depends on four indexes: we can identify two indexes related to the basis functions expansions (say, N_z and N_ϕ, the subscript being related to coordinates z and ϕ, respectively), and two indexes related to series (7)–(10) (say, M_z and M_ϕ). It was observed that $N_\phi = 5$ yields very good results in all cases. In order to show some partial results on the convergence properties of the method, we have focused on parameter S_{11} (in decibels) obtained by varying index N_z for a two port-structure. The results are presented in Fig. 3, where convergence is compared with accurate measurements carried out at the Centro Studi per le Telecomunicazioni Spaziali (CSELT), Milan, Italy ($N_\phi = 5$ and large values of M_z and M_ϕ were used). The parameter shown in this figure on the horizontal axis is actually the *maximum* index along z, computed for $h = a$. At internal

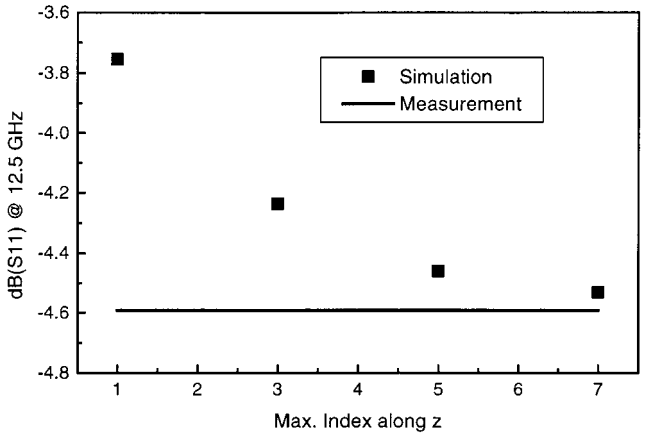

Fig. 3. Convergence of parameter $|S_{11}|$ (in decibels) for two facing posts ($r_1 = r_2 = 7.5$ mm, 4- and 2-mm height, respectively) in a rectangular waveguide WR75 (center-band frequency).

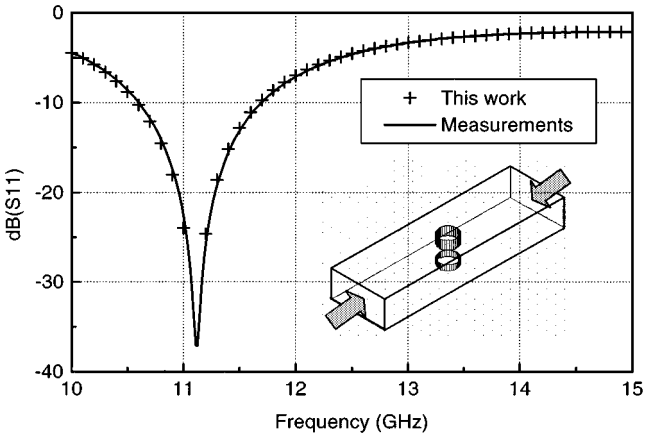

Fig. 4. Two-port network: comparison between measured and simulated S-parameters. Two facing posts having $r_1 = r_2 = 7.5$ mm, 4- and 2-mm height, respectively in a rectangular waveguide (WR75).

cylindrical cavity regions having $h < a$, smaller values of N_z were used. Also in this case, a maximum index $N_z = 5$ represents a good tradeoff between speed of analysis and accuracy. As a general rule, the choice of indexes M_z and M_ϕ can be carried out as follows:

$$M_z = N_z + M_z'$$

$$M_\phi = N_\phi \frac{\theta}{2\pi} + M_\phi'$$

where M_z' depends on the geometry and M_ϕ' is a fixed parameter (obtained simply by observing the global convergence of the method). The figure corresponds to two facing posts of the same radius (7.5 mm) and of 4- and 2-mm heights, respectively, and the frequency is the center-band frequency in the rectangular waveguide used. The complete comparison between measured and simulated data for the previous post is shown in Fig. 4.

In Fig. 5, a two-port network consisting of two reentrant posts (sketched in the same figure) is shown. The inset structure consists of a cylindrical post partially inserted in a second hollow cylindrical post, both inserted in a waveguide. The waveguide has $a = 15$ mm and $b = 30$ mm. The smaller post has 2-mm radius and 10-mm height. The larger post has 6-mm

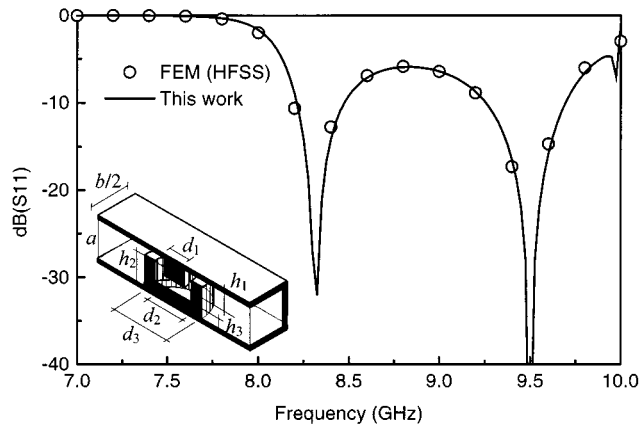

Fig. 5. Two-port network: comparison between simulated S-parameters by the method in this paper and by the FEM (Hewlett-Packard HFSS program). Two reentrant posts (one-half of the structure is shown in this figure) having $d_1 = 4$ mm, $h_1 = 10$ mm, $d_2 = 8$ mm, $d_3 = 12$ mm, $h_2 = 10$ mm, and $h_3 = 3$ mm in a rectangular waveguide ($a = 15$ mm, $b = 30$ mm).

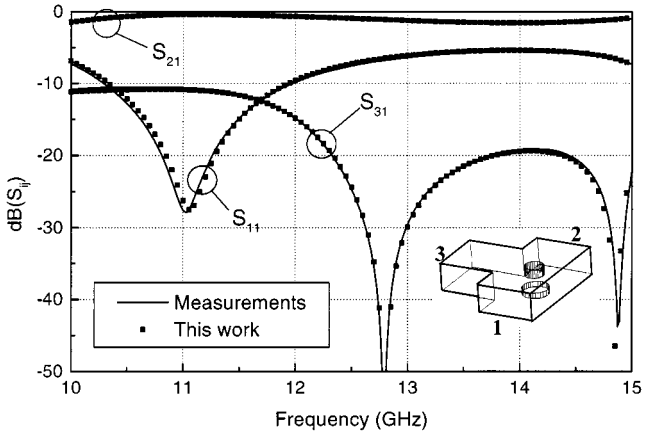

Fig. 6. Three-port network: 90° T-junction between three WR75 waveguides with a cylindrical inset consisting of two facing posts having $r_1 = 7.5$ mm, $r_2 = 2.5$ mm, $h_1 = 4.06$ mm, and $h_2 = 2.06$ mm. Comparison between measurements and simulations.

radius and 10-mm height, and a metal thickness of 2 mm. The analysis was applied by dividing the structure in four regions (see Fig. 1). The figure compares the results obtained in this paper with those of finite elements (Hewlett-Packard HFSS program). The agreement is good, although convergence of the finite-element method (FEM) was observed as being rather slow.

A further example is shown in Fig. 6. In this case, a three-port structure is shown and the results obtained by this method are compared with measurements on a test prototype built for validation purposes. The prototype comprises two facing posts (of 15- and 5–mm diameter and 4.06- and 2.06-mm height, respectively) centered in a 90° T-junction between three WR75 waveguides. S-parameters have been measured two by two by connecting a matched load to either ports of the structure. The agreement between measurements and simulation is good and the small differences may be ascribed to small mechanical tolerances in the post alignment and/or location.

IV. Conclusion

A new GAM approach for the multiport analysis of rectangular waveguides/resonators loaded by arbitrary circular rods insets has been presented in this paper. The method is based on the combination of two efficient techniques that solve the full 3-D problem by reducing it to a set of uncoupled 2-D problems. The internal structure has been solved by a new radial GAM approach, combining flexibility, accuracy, and good efficiency. The method has been validated by comparing the results found with measured and simulated (by FEM) data for two- and three-ports structures.

Acknowledgment

The author would like to thank L. Accatino, Centro Studie Laboratorie Telecommunicazioni S.p.A. (CSELT), Turin, Italy, and G. Bertin, CSELT, Turin, Italy, for their kind and competent cooperation. Measurements for this paper were conducted at the CSELT Microwave Laboratory, Turin, Italy.

References

[1] H.-W. Yao, K. A. Zaki, A. E. Atia, and R. Hershtig, "Full-wave modeling of conducting posts in rectangular waveguides and its applications to slot-coupled combline filters," *IEEE Trans. Microwave Theory Tech.*, vol. 43, pp. 2824–2830, Dec. 1995.

[2] V. Boria, G. Gerini, and M. Guglielmi, "Computer aided design of reentrant coaxial filters including coaxial excitation," in *IEEE MTT-S Int. Microwave Symp. Dig.*, vol. 3, 1999, pp. 1131–1134.

[3] J. A. Brandshow, "Scattering from a round metal post and gap," *IEEE Trans. Microwave Theory Tech.*, vol. MTT-21, pp. 313–322, May 1973.

[4] Y. Huang, N. Yang, S. Lin, and R. F. Harrington, "Analysis of a post with arbitrary cross-section and height in a rectangular waveguide," *Proc. Inst. Elect. Eng.*, pt. H, vol. 138, pp. 475–480, Oct. 1991.

[5] G. G. Gentili and A. Melloni, "Analysis of the X junction between two rectangular waveguides and a circular waveguide," *IEEE Microwave Guided Wave Lett.*, vol. 7, pp. 245–247, Aug. 1997.

[6] G. G. Gentili, R. Nesti, and G. Pelosi, "Efficient analysis of a complete feeding system in corrugated circular waveguide," *J. Electromag. Waves Applicat.*, vol. 13, pp. 1631–1648, 1999.

[7] P. C. Sharma and K. C. Gupta, "Desegmentation method for analysis of two-dimensional planar circuits," *IEEE Trans. Microwave Theory Tech.*, vol. MTT-29, pp. 1094–1098, Oct. 1981.

Gian Guido Gentili was born in Turin, Italy, in 1961. He received the Laurea degree in electronics engineering from the Politecnico di Milano, Milan, Italy, in 1987.

In 1989, he joined the Centro Studi per le Telecomunicazioni Spaziali, National Research Council (CSTS-CNR), Politecnico di Milano, where he is currently a Senior Researcher and also teaches an electromagnetics fields course. His main research interests are concerned with the application of numerical methods to electromagnetic problems, including complex waveguide circuits, microstrip patch antennas and coupled lines, horn antennas, and ground penetrating radar. In 1993 and 1995, he was Visiting Scientist at the Politecnica of Madrid, Madrid, Spain.